JAAS

Detection of hydrogen isotopes in Zircaloy-4 via femtosecond LIBS

Journal:	*Journal of Analytical Atomic Spectrometry*
Manuscript ID	JA-ART-01-2021-000034.R1
Article Type:	Paper
Date Submitted by the Author:	31-Mar-2021
Complete List of Authors:	Kautz, Elizabeth; Pacific Northwest National Laboratory Ronnebro, Ewa; Pacific Northwest National Laboratory, Devaraj, Arun; Pacific Northwest National Laboratory Senor, David; Pacific Northwest National Laboratory Harilal, Sivanandan; Pacific Northwest National Laboratory

ARTICLE

Detection of hydrogen isotopes in Zircaloy-4 via femtosecond LIBS

Elizabeth J. Kautz,[a]* Ewa C.E. Rönnebro,[a] Arun Devaraj,[a] David J. Senor,[a] and Sivanandan S. Harilal[a]*

Received 00th January 20xx,
Accepted 00th January 20xx

DOI: 10.1039/x0xx00000x

The analysis of hydrogen isotopes (^{1}H, ^{2}H, and ^{3}H) is crucial to several applications, including nuclear forensics and safeguards, characterization of nuclear fission and fusion reactor materials, geochemistry, and space exploration. Laser-induced breakdown spectroscopy (LIBS) is a promising tool for the real-time analysis of hydrogen isotopes. However, the accurate, quantitative analysis via LIBS can be challenging due to ^{1}H contamination on sample surfaces, residual ^{1}H in the analysis environment, minor amounts of solute ^{1}H, and spectral line broadening. Here, we characterize femtosecond laser induced plasmas from Zircaloy-4 targets with varying ^{1}H and ^{2}H concentrations in a He gas environment via spatially and temporally resolved optical emission spectroscopy. The impact of varying ambient gas pressure, the spatial distribution, and temporal histories of species viz., $^1H_\alpha$, $^2H_\alpha$, and Zr I on Zircaloy-4 plasma spectral features are reported. $^1H_\alpha$ and Zr I emission features are found to have different ambient pressure dependencies and are separated in both space and time in the laser induced plasmas. Lastly, the measured $^2H_\alpha$ emission intensities for a wide range of ^{2}H concentrations in Zircaloy-4 samples showed a linear trend when plotted versus known ^{2}H concentration.

I. Introduction

Hydrogen is the most abundant element in the universe and can be harnessed and used in energy and defence applications. However, the pervasive nature of hydrogen combined with its fast diffusivity can also be detrimental to material performance. Therefore, detection and analysis of hydrogen isotopes, i.e., protium (^{1}H), deuterium (^{2}H) and tritium (^{3}H), are central to several application areas ranging from nuclear energy and forensics to geochemistry and space exploration.[1-3] The detection and accurate quantification of ^{1}H, ^{2}H, and ^{3}H is an important aspect of materials characterization efforts needed for monitoring the ^{1}H or ^{2}H picked up by nuclear reactor fuel cladding (e.g., Zircaloys and other Zr-based alloys commonly used in pressurized and boiling water reactors)[4] during the waterside corrosion process, and ^{3}H retained in plasma-facing components of fusion reactors.[5-7] The detection of hydrogen and hydrogen-containing compounds is also needed for identifying and assessing aqueous environments and their habitability in remote locations, such as on Mars.[2] However, the quantitative analysis of ^{1}H, ^{2}H, and ^{3}H is a complex problem. Several specialized mass spectrometry techniques are often employed, including (but not limited to): isotope ratio mass spectrometry (IR-MS), inductively coupled plasma mass spectrometry (ICP-MS), time of flight SIMS (ToF-SIMS), nanoscale secondary ion mass spectrometry (NanoSIMS), and atom probe tomography (APT).[8-12] Some of these techniques are capable of mapping isotopic abundances in nanoscale volumes (e.g., NanoSIMS, APT[13]), others are capable of detecting trace amounts of isotopes (i.e. ICP-MS), and therefore can provide unique insights into material condition and ^{1}H, ^{2}H, or ^{3}H ingress mechanisms. Yet, there are significant challenges in the application of these methods, namely: the inability to perform analysis at standoff distances, the need for complex and time-consuming sample preparation, limited field of view (for certain microscopy methods), and the inability to reliably separate residual hydrogen in the analytical environment from solute hydrogen.

Laser-induced breakdown spectroscopy (LIBS) is a method routinely used for the analysis of elements and some isotopes.[14-16] LIBS is a versatile technique with many advantages over specialized laboratory-based mass spectrometry methods, such as the ability to perform rapid, *in situ* multi-elemental (or isotopic) analysis, no sample preparation requirement, relatively simple experimental set-up (and the possibility to make portable), and the ability to analyse targets in the solid, liquid, or gas phase.[17-19] The analysis of ^{1}H and ^{2}H in various target materials (e.g., ^1H_2O, ^2H_2O, minerals, metals, alloys) has previously been performed using LIBS employing a variety of laser ablation (LA) schemes and optical emission spectroscopy tools.[19-24] Plasmas produced from a solid ^2H_2O-^1H_2O target in air were studied and a double pulse configuration with a short inter-pulse delay (50 ns) was proposed for improving $^2H_\alpha$ and $^1H_\alpha$ line intensity and reducing Stark broadening.[20] In an effort to reduce line broadening of Balmer $^2H_\alpha$ and $^1H_\alpha$ lines in atmospheric pressure environments, an orthogonal dual-pulse set-up was proposed, involving the separate ablation of a Zircaloy-4 target and He gas to generate two plasmas.[25] The emission spectra collected using this method showed a clear separation between $^2H_\alpha$ and $^1H_\alpha$ lines, and a detection limit of 20 µg/g was achieved. A He gas environment was again employed for the analysis of ^{2}H in Zircaloy-4 and other light isotopes[26] to take advantage of the so-called He-assisted excitation process,[27] and a 10 ppm ^{2}H detection limit was reported. A fs-filament has also been used to generate plasmas from ^1H_2O and ^2H_2O targets, which produced low temperature,

[a] *Address here.*
[b] *Address here.*
[c] *Address here.*
† Footnotes relating to the title and/or authors should appear here.
Electronic Supplementary Information (ESI) available: [details of any supplementary information available should be included here]. See DOI: 10.1039/x0xx00000x

low-density plasmas advantageous for reducing the $^1H_\alpha$ line broadening in the laser induced breakdown (LIB) plasma, and is also ideal for standoff measurements.[22] Various calibration methods were tested in order to develop a calibration-free protocol for predicting ^2H concentration from an emission spectrum.[22] The isotopic shift between $^{16}O^1H$ and $^{16}O^2H$ molecules have also been employed to detect ^1H and ^2H via LIBS, which can be advantageous due to the large isotopic shift (0.68 nm), and reduced Stark broadening in comparison to $^1H_\alpha$ and $^2H_\alpha$ lines.[28, 29]

In our recent work, we investigated the impact of plasma generation conditions (i.e., nanosecond versus femtosecond LA) and the nature of the ambient inert gas (i.e., Ar versus He) on emission spectral features of Zircaloy-4 plasmas.[30] Time-resolved, two-dimensional spectral imaging was performed to map the spatial and temporal behaviour of $^1H_\alpha$, $^2H_\alpha$, and Zr I species in the plume. The nature of the ambient gas was found to impact both plasma confinement and physical conditions (i.e., temperature, electron density) in ns and fs LIB plasmas. An Ar ambient led to better confinement, and hence hotter, denser plasmas. Hotter plasma conditions in Ar were attributed to energy transfer from metastable energy levels to analytes via collisional energy transfer.[31] Greater confinement and temperatures in an Ar gas (compared to He) led to larger $^2H_\alpha$ and $^1H_\alpha$ linewidths due to Stark and Doppler broadening. The presence of lighter He gas with high thermal conductivity helped to effectively cool the plasma,[26] reducing temperature and electron density, and thus providing narrower linewidths. The use of femtosecond (fs) LA was also identified as advantageous (in comparison to LA using traditional long pulse, i.e., ns lasers) due to improved spatial resolution, better control for depth profiling, and possibility to achieve minimal heat-affected zones.[32]

Although LIBS is a promising technique for the detection of ^1H, ^2H, and ^3H in both laboratory and standoff measurement configurations, there are still many challenges to overcome. A key parameter in the application of isotopically-resolved LIBS is line broadening relative to the isotopic shift (0.18 nm for $^1H_\alpha$ and $^2H_\alpha$, and 0.23 nm for $^1H_\alpha$ and $^3H_\alpha$). In order to reduce line broadening, improve peak separation, and have a strong emission signal, several factors must be considered, including the trade-off between long integration times, delay time with respect to plasma onset and rapidly decaying emission signal, ambient gas pressure, and the spatial segregation of plume species. The spatial segregation of species may become increasingly important in the analysis of multi-component targets such as alloys, natural minerals, or rocks. Thus, a comprehensive understanding of the role of the experimental parameters impacting the detection of ^1H, ^2H, and ^3H via fs LIBS is needed. Here, we study the role of ambient gas pressure and species segregation (in both space and time) in the analysis of ^1H and ^2H via fs LIBS. We analyse Zircaloy-4 targets with varying ^2H concentrations in a He gas environment. He gas background pressure was varied between ~3 – 250 Torr to investigate the impact of pressure on spectral features, emission intensity, line broadening, signal-to-background and signal-to-noise ratios. Spatially and temporally resolved spectral features were collected to map emission intensity and line broadening and estimate time-dependence of electron density. Lastly, spatially and temporally resolved photomultiplier signal emission profiles, also referred to as time of flight spectroscopy or optical time of flight (OTOF),[33-37] was performed to investigate the spatio-temporal relationship of $^2H_\alpha$ and Zr I emission in the LIB plasma.

II. Experimental Details

Zircaloy samples with varying ^1H and ^2H concentrations up to 41 at. % (~15,200 ppm by mass) were used in the present experiment. For sample preparation, ^1H or ^2H was absorbed into Zircaloy-4 samples using a custom-built high vacuum system briefly described here. A ~1-2 cm section of Zircaloy-4 tube (~100 µm thick) was weighed using a calibrated analytical balance to an estimated uncertainty of 0.5 mg to compare to weight after ^1H or ^2H absorption. The Zircaloy-4 section was placed in a quartz tube that is enclosed in a furnace. The quartz tube is connected to stainless steel tubing using a glass-metal transition to seal it and thereafter evacuated to high-vacuum before a leak test was performed. $^1H_2$ or $^2H_2$ gas was then inserted into the system by using a calibrated capillary leak on a $^1H_2$ or $^2H_2$ gas bottle (99.999 %, ultra high purity) with a leak-rate of 2.6×10^{-8} mol/s. Time needed to reach a certain concentration (at. %) of ^1H or ^2H was estimated based on the leak rate. The furnace was heated up under dynamic vacuum to remove any impurities in the system, and a thermocouple on the outside of the quartz tube recorded the temperature to be 525 °C. After heating to the 525 °C test temperature, the $^1H_2$ or $^2H_2$ gas was inserted into the quartz tube and pressure was monitored with a capacitance manometer (< 10 Torr). After the desired test time elapsed (based on target ^1H or ^2H concentration), the specimen was removed from the furnace and weighed to confirm how much ^1H or ^2H was absorbed. During $^1H_2$ or $^2H_2$ gas exposure, ^1H or ^2H is in solid solution with Zr (α-phase) below 5 at. % and at higher concentrations, a hydride phase is precipitated (in this case, the δ-phase). An example microstructure of Zircaloy-4 after hydride phases have precipitated is illustrated in the Fig. 1 micrograph for a ^2H concentration of ~ 41 at. %. This micrograph was taken using a Thermo Fisher Quanta 3-D dual beam focused ion beam, scanning electron microscope (FIB-SEM), using the backscatter electron detector. The darker contrast ^2H-rich phase is distributed along Zircaloy-4 grain boundaries. Grain diameters are approximately ~5-10 µm, and the laser spot size selected for analyses (~500 µm) ensures material from multiple Zircaloy-4 grains and ^1H or ^2H-rich secondary phases are ablated. Thus, the ^1H or ^2H concentration analysed in the plasma is considered to be representative of the bulk composition, after any residual ^1H on the sample surface is removed.

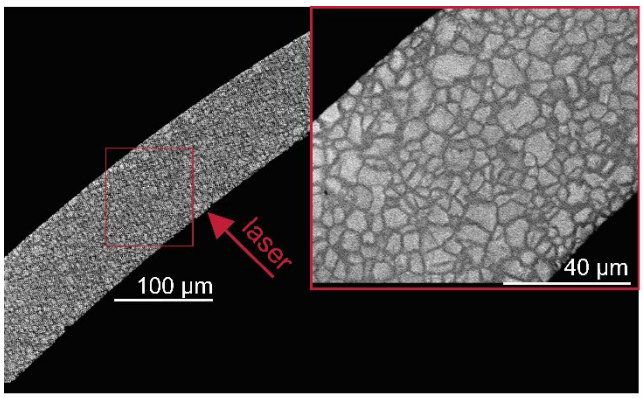

Fig. 1. Zircaloy-4 microstructure with ~ 41 at. % ^{2}H. Micrograph was taken using the backscatter electron detector for showing the distribution of the darker ^{2}H-rich phase along Zircaloy-4 grain boundaries. This micrograph is taken of a cross-section of a Zircaloy-4 tube, and the orientation of the incident laser (on the inner diameter) used in this work is shown with a red arrow. The figure inste shows a higher magnification of the Zircaloy-4 microstructure.

For plasma generation, pulses from a Ti:Sapphire laser (Coherent Astrella) with 800 nm wavelength, ~35 fs FWHM, operated at 10 Hz, with a laser pulse energy of ~5.0 mJ was used. As shown in Fig. 1, the laser was focused onto the inner diameter of a section of Zircaloy-4 tube. A fluence of ~ 2.5 J/cm^{2} was used for generating plasmas. Zircaloy-4 targets were mounted in a cubic vacuum chamber (0.004 m^{3}) for analysis. The chamber was placed on a x-y-z translator to easily move between targets, and to prevent drilling. Optical windows for laser entrance and light collection were included in the chamber design. A pressure gauge, vacuum pump, and a gas line were also attached to the chamber to control ambient gas pressure. High purity He gas (~99.998 %) was used in experimentation. Three Zircaloy-4 samples were used to investigate the optimal parameters for analysis, including: (1) ~38 at. % ^{2}H, (2) ~38 at. % ^{1}H, and (3) no ^{1}H or ^{2}H loading (i.e., in the as-received condition). For comparing measured $^{2}H_{\alpha}$ emission to known ^{2}H concentration, five different Zircaloy-4 samples with varying ^{2}H concentration ranging from ~2 – 41 at. % were analysed. ^{1}H is present in the as-received and ^{2}H-containing samples as a trace element with an expected concentration of ~25 ppm. ^{1}H is also present as an impurity on sample surfaces.

For analysing emission from laser induced plasmas, an optical system consisting of two plano-convex lenses was used for imaging the plasma plume onto the slit of a 0.5 m Czerny Turner spectrograph (SpectraPro), equipped with two detectors: an intensified charged coupled device (ICCD, Princeton Instruments PiMAX4) and a photomultiplier tube (PMT, Hamamatsu R955) with a ~2 nanosecond rise time. A diverter mirror was used for selecting the detector for analysis. The optical emission spectroscopic system was positioned orthogonal to the plasma expansion direction. The spectrograph provided a spectral resolution of ~ 0.020 nm, measured using a 632 nm He–Ne laser and a 2400 grooves per mm grating. This same grating was used for all data collection. Spatially resolved spectra were collected to track the spatial distribution of H isotopes and other species within the plume. The monochromator-PMT system was used for measuring the emission at varying distances from the target for spatially and temporally resolved analyses.

III. Results and Discussion

a. Surface contamination and cleaning

The Balmer series consists of three strong emission lines in the visible spectrum: $^{1}H_{\alpha}$ (656.28 nm), $^{1}H_{\beta}$ (486.14 nm), and $^{1}H_{\gamma}$ (434.05 nm). Each α, β, and γ line has a different isotopic shift between ^{1}H and ^{2}H (0.180 nm, 0.135 nm, and 0.119 nm for α, β, and γ, respectively), in addition to varying characteristics such as asymmetric line profiles, broadening, etc.[38, 39] $^{1}H_{\alpha}$ has the smallest Stark line broadening with a larger isotopic separation between $^{1}H_{\alpha}$ and $^{2}H_{\alpha}$. For these reasons, the $^{1}H_{\alpha}$ and $^{2}H_{\alpha}$ line at 656.28 nm and 656.10 nm, respectively, are the focus of this work, referred to here simply as $^{1}H_{\alpha}$ and $^{2}H_{\alpha}$.

The spectral region selected for analysis is 653.31-658.63 nm, which contains $^{1}H_{\alpha}$ and $^{2}H_{\alpha}$ lines along with several Zr atomic and ionic transitions. For detecting ^{1}H or ^{2}H using any analytical technique, the issue of ^{1}H existing as a contaminant on the sample surface or its presence in the analysis environment is an important consideration. To preclude any ^{1}H surface contamination, several laser cleaning shots were fired and spectra were averaged for every two shots. Here, the as-received and ^{2}H-loaded (~ 38 at. %) samples were compared in order to determine how the presence of any ^{1}H surface contamination may impact detecting the isotopic shift, and also to compare $^{1}H_{\alpha}$ emission signal intensity in the ^{2}H-loaded and as-received conditions, since the ^{1}H concentrations are expected to be similar.

Figs. 2(a) and 2(b) show emission spectra for as-received and ^{2}H-containing Zircaloy-4 targets, respectively, as a function of laser shots. All spectra were taken at a distance of 2 mm from the target. In both Fig. 2(a) and (b), $^{1}H_{\alpha}$ emission intensity is significantly higher (by a factor of ~4-8) for the initial laser shots, and after several shots (~8) the $^{1}H_{\alpha}$ emission is approximately constant for subsequent shots. This trend is clearly highlighted in Fig. 2(c). The difference in emission intensities of $^{1}H_{\alpha}$ for the initial laser shots in as-received versus ^{2}H-containing samples is attributed to differences in ^{1}H contamination present on these two different sample surfaces. In addition, we find that for the ^{2}H-containing sample, the $^{2}H_{\alpha}$ emission intensity reaches a steady state value after several shots (~20-30). Hence, several laser 'cleaning' shots are needed to remove ^{1}H contamination, and to reach a steady-state emission signal intensity for the analyte of interest prior to performing any analysis of bulk ^{1}H or ^{2}H concentrations. It is important to note that the number of cleaning shots needed is highly dependent on laser fluence and the sample condition (i.e., the amount of ^{1}H on the sample surface as an impurity). At the laser fluence used here, removal of ^{1}H from the sample surface is efficiently performed in the first several shots, and hence no additional sample heating or surface preparation was required. In prior work, most of the surface ^{1}H contamination was removed by heating the analytical environment (i.e., sample chamber) in vacuum to 150 °C for 30 minutes.[40]

It is also important to note that the intensity of the $^1H_\alpha$ line present in the ^{2}H-containing sample emission spectrum (Fig. 2(b)) matches well with the emission intensity of $^1H_\alpha$ in the as-received sample (Fig. 2(a)). We attribute this $^1H_\alpha$ emission signal primarily to solute ^{1}H present as a trace impurity in Zircaloy-4. Minor amounts of ^{1}H present in the analysis environment may also contribute. However, their contribution should be similar for all targets studied regardless of the cleaning shots.

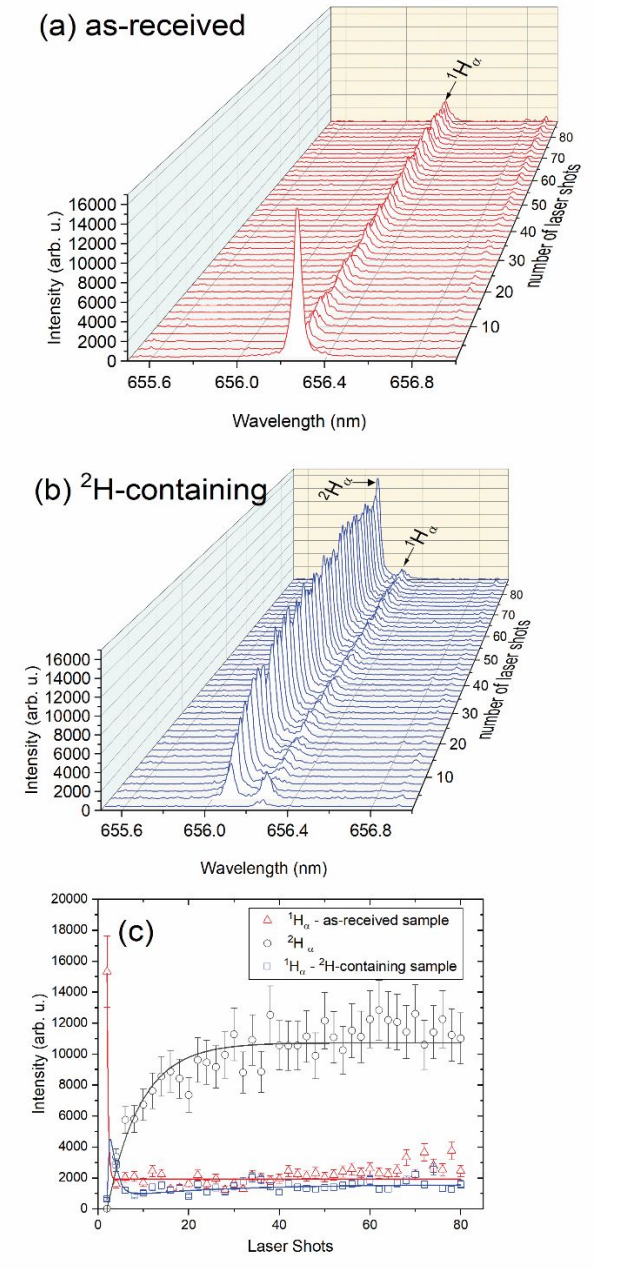

Fig. 2. Spectral features for (a) as-received and (b) ^{2}H-containing Zircaloy-4 targets in a 10 Torr He gas environment, with (c) emission intensity versus number of laser shots for $^1H_\alpha$ in the as-received sample, $^1H_\alpha$ in the ^{2}H-containing sample, and $^2H_\alpha$. All spectra were collected at 2 mm from the target using a gate delay/width of 600 ns/1 µs.

b. Pressure effects

The presence of an inert ambient gas is often used in LIBS for avoiding plasma chemistry and improving the analytical merits.[17] It is well established that the nature of the ambient gas significantly impacts LIB plasma emission intensity and properties.[41, 42] In addition, plasma generation conditions can significantly impact spectral features and plasma physical properties.[43] Our prior work demonstrated fs LA in a He gas environment led to a lower temperature and density plasma, in comparison to ns LA and in an Ar ambient, and hence is well-suited for the analysis of ^{1}H and ^{2}H.[30] Here, we further explore the effects of He ambient gas pressure on spectral features of plasmas produced from ^{1}H-loaded Zircaloy-4. Since similar broadening and spatial distributions of ^{2}H and ^{1}H were observed, the ^{1}H-loaded sample was used for several analyses. Plasmas produced from ^{2}H-loaded Zircaloy-4 are expected to show similar trends, and ^{2}H-loaded samples are studied here in subsequent sections. Owing to the significant variability in emission spectral features with distance from the target and in time after plasma onset, spatially and temporally-resolved data are used in the present study.

Spectral features from a ^{1}H-containing Zircaloy-4 sample for varying He pressures from 3.5 – 250 Torr are presented in Fig. 3 at a distance of ~ 0.5 mm from the target using a gate delay/width of 300 ns/200 ns. Prominent Zr and H emission lines in the spectral region are labelled. The energy levels of various transitions in the spectral window of interest to this study are: Zr I at 655.05 nm (26902.450 → 11640.720 cm-1), 2Hα at 656. 10 nm (97518.841→82281.662 cm-1), 1Hα at 656.28 nm (97492.302 →82259.105 cm-1), Zr I at 656.95 nm (20466.830 →5249.070 cm-1), and Zr II at 657.8650 (34810.030 → 19613.540 cm-1).[44] At pressures of ~ 3.5-40 Torr, Zr I and Zr II emission is found to be very weak in comparison to $^1H_\alpha$. The increase in Zr I and reduction in $^1H_\alpha$ emission intensities with respect to ambient pressures greater than ~40 Torr is due to plasma cooling. Previous studies highlighted that temperature of the plasma decays with increasing background pressure.[45] The Zr I emission lines in the selected spectral window originated from lower energy levels compared to $^1H_\alpha$ emission. Hence, higher excitation energy is required for $^1H_\alpha$ emission.

The emission intensity, full width half maximum (FWHM) signal to background ratio (SBR), and signal to noise ratio (SNR) of $^1H_\alpha$ were measured for comparing spectral emission features as a function of He pressure. The emission intensities of $^1H_\alpha$ and Zr I (655.05 nm) lines were measured by taking the area of a Voigt fit and are reported in Fig. 4 along with FWHM. Fig. 5 reports SBR and SNR for $^1H_\alpha$ for a ^{1}H-containing Zircaloy-4 target. SBR and SNR were calculated using the maximum intensity of $^1H_\alpha$ line (I_{max}), the averaged background intensity ($I_{background}$) on higher and lower wavelength sides of the $^1H_\alpha$ line, and the standard deviation of the background ($\sigma_{background}$), according to Equations (1) and (2)[46]:

$$\frac{S}{N} = \frac{I_{max} - I_{background}}{\sigma_{background}} \quad (1)$$

$$\frac{S}{B} = \frac{I_{max}}{I_{background}} \quad (2)$$

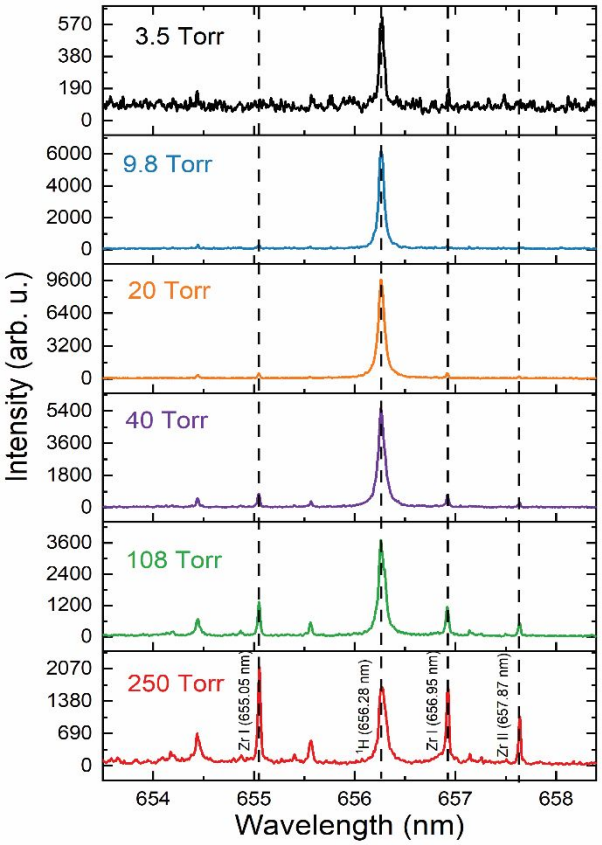

Fig. 3. Spectral features of a LIB plasma produced from a ^{1}H-containing Zircaloy-4 sample in varying He pressures. All measurements were taken at a distance of ~0.5 mm from the target, using a gate delay/width of 300 ns/ 200 ns. Each spectrum was averaged over 12 shots.

From Fig. 4(a), we find that emission intensity of $^1H_\alpha$ peaks at moderate He pressures, whereas Zr I emission intensity increases with pressure. Fig 4(b) shows that FWHM of the $^1H_\alpha$ follows an approximately linear trend and increases with pressure. Similar to the trend in $^1H_\alpha$ emission intensity, $^1H_\alpha$ SBR reaches a maximum at moderate He pressure levels (~20-30 Torr), shown in Fig. 5(a), then decreases with increasing pressure. $^1H_\alpha$ SNR (Fig 5(b)) peaks at similar pressure levels. Given that linewidth to line separation is the most crucial consideration for isotopic analysis employing optical spectroscopic tools,[18] the line broadening mechanisms contributing to the measured FWHM of the $^1H_\alpha$ line are scrutinized. The lowest measured $^1H_\alpha$ linewidth is ~ 60 pm at ~10 Torr pressure level, and it increases with increasing He pressure level. Several factors contribute to the FWHM of $^1H_\alpha$ observed in the Fig. 3 spectra and reported in Fig. 4(b), including the fine and hyperfine structure components, instrumental broadening (~20 pm), Stark, Doppler, natural, and pressure. In this system, natural and pressure broadening are negligible compared to the other broadening mechanisms. Stark broadening is prominent in the early times of plasma evolution.[18] Line broadening caused by the Stark effect, which has a Lorentzian line shape, is due to the presence of the electric field generated by the charged particles in the plasma. Since the Stark effect for ^{1}H varies linearly with the electric field[47], it has a significant effect on linewidth even at later times in the plasma lifecycle. In addition to Stark, the Doppler effect is also significant for ^{1}H since it is the lightest element in the periodic table. Doppler broadening has a Gaussian line shape and scales with the square root of temperature,[18] and therefore may be more significant at higher plasma temperatures. Lastly, the instrumental broadening will be present in all emission spectroscopy set-ups, varies from system to system, and depends on the spectrometer dispersion, slit width, detector pixel width, spectrograph aberrations, alignments, etc. Hence the recorded spectral profiles represent a convolution of several broadening effects that are prominent at different times in plasma evolution. Fine and hyperfine splitting of ^{1}H and ^{2}H electronic energy levels also contributes to the measured line widths. The splitting of electronic levels is a result of spin-orbit coupling and electron-nuclear spin-spin interaction. Hyperfine structure components span ~20 pm for both $^1H_\alpha$ and $^2H_\alpha$,[22] and Stark and Doppler broadening mechanisms affect each fine structure component. The hyperfine splitting of ^{1}H and ^{2}H spectral lines have been studied both experimentally and theoretically by several authors[48-51], and details of hyperfine structures are summarized in a compilation by Kramida.[49]

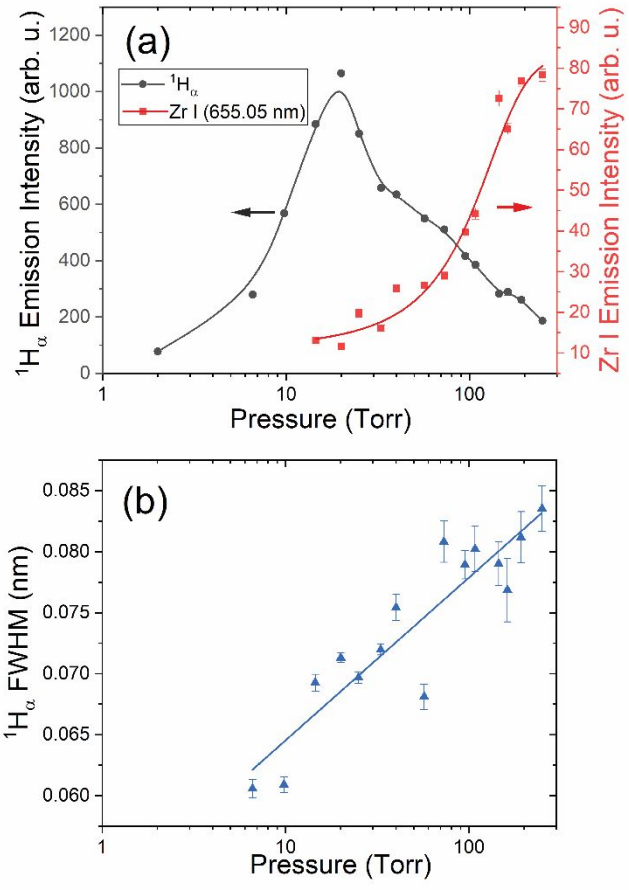

Fig. 4. Variability of (a) emission intensity of ^{1}H (656.28 nm) and Zr I lines (655.05 nm), (b) ^{1}H SBR, and (c) ^{1}H FWHM, and as a function of He pressure from ~3-250 Torr. Results are determined from analysis of an ^{1}H-containing Zircaloy-4 sample. All experimental parameters used for data collection are given in the Fig. 2 caption. Curves in each sub-figure are provided as a guide for the eye.

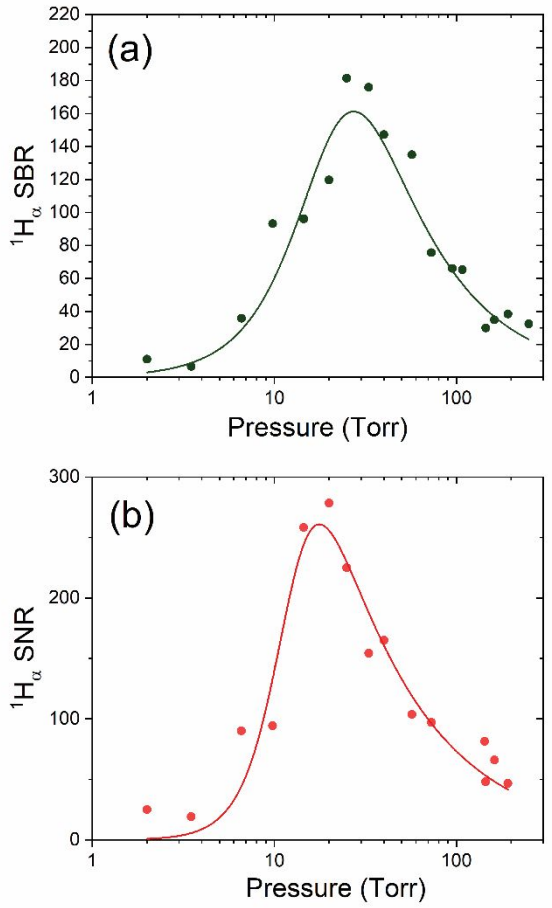

Fig. 5. Variability of (a) $^1H_\alpha$ SBR, and (b) $^1H_\alpha$ SNR as a function of He pressure from ~3-250 Torr. Results are determined from analysis of an ^1H-containing Zircaloy-4 sample. All experimental parameters used for data collection are given in the Fig. 2 caption. Curves in each sub-figure are provided as a guide for the eye.

Over the pressure range studied, the relative contributions of different broadening mechanisms vary. At moderate to higher pressures (up to ~100 Torr), the line shape is found to be primarily Lorentzian, indicating that Stark broadening is the dominant mechanism. This is not surprising since the spectral measurements were carried at early times of plasma evolution (300 ns gate delay). Overall, Fig. 4 and 5 highlight important trade-offs in the analysis of $^1H_\alpha$, namely: increasing pressure leads to greater $^1H_\alpha$ emission intensity and better SBR and SNR, but also leads to increased line broadening. Further analysis of Zircaloy-4 spectral features at varying distances from the target and at different times in fs LIB plasma evolution are needed to identify the best parameters (i.e., pressure, distance, time) for $^1H_\alpha$, $^2H_\alpha$, or $^3H_\alpha$ analysis in a multi-component plasma. Based on pressure effect studies, the 10-20 Torr He pressure range is suitable for analysis. Thus, further spatial and temporal analyses were carried out in this moderate pressure regime.

c. Spatially resolved spectral features

Spatially resolved spectral features from a ^1H-containing Zircaloy-4 plasma are shown in Fig. 6(a) at 600 ns after plasma onset in 10 Torr He, with corresponding spatially resolved emission intensities for ^1H and Zr I given in Fig. 6(b). From Fig. 6(a), we find $^1H_\alpha$ and Zr I emission intensities are spatially segregated in the plasma: H I emission is stronger closer to the target, whereas Zr I emission is prominent at farther distances. Fig. 4(b) clearly demonstrates this trend, showing that $^1H_\alpha$ emission intensity is maximum ~0.5 – 1.0 mm from the target, whereas Zr I emission intensity peaks ~ 2.5 mm from the target. This trend indicates $^1H_\alpha$ emission is prominent when the temperature of the plasma system is higher (closer to the target) while Zr I emission lines become predominant in cooler regions of the plasma. These emission intensity changes with distance can be correlated to the upper energy levels of selected transitions. For example, the upper energy level of $^1H_\alpha$ emission is 97492.302 cm^{-1} (~12 eV), while the Zr I and II emission lines originated from 20466.830 - 34810.030 cm^{-1} (~2.5 - 4.3 eV). The high thermal conductivity He gas environment is responsible for the effective plasma cooling at the plume edges, and at distances farther from the target, as the plasma rapidly expands after onset. The measured FWHM of $^1H_\alpha$ is given in Fig. 6(c), and shows the FWHM is lowest at closer and farther distances from the target, and the maximum broadening is observed at ~2.5 mm. This trend indicates that contributions to the line broadening (i.e., Stark, Doppler) depend strongly on space and time. Hence, time-resolved analysis of spectral features were carried out.

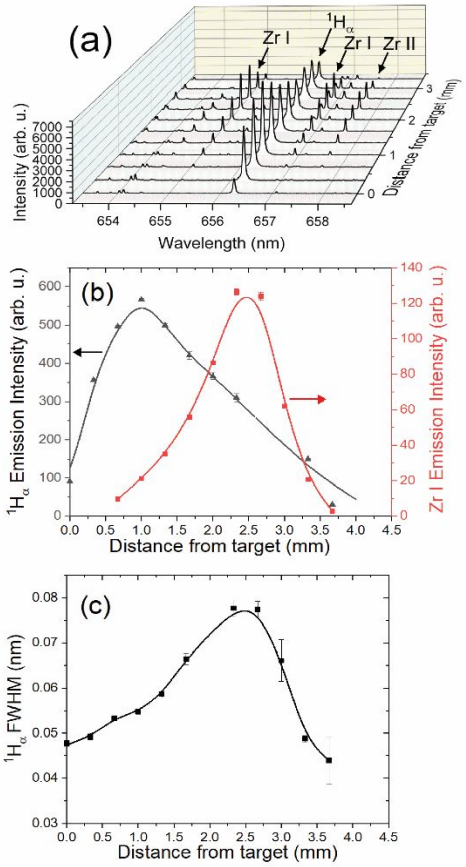

Fig. 6. (a) Spatially resolved spectral features of a plasma produced from a ^1H-containing Zircaloy-4 target in 10 Torr He gas environment using a gate delay/width of 600 ns /1 µs. (b) Emission intensity of $^1H_\alpha$ and Zr I (655.05 nm) at increasing distances from the target. (c) FWHM of $^1H_\alpha$ as a function of distance from the target.

d. Temporal evolution of $^1H_\alpha$ and Zr I emission intensities, linewidth, and electron density

In addition to the spatial analysis of emission features, the temporal evolution of $^1H_\alpha$ and Zr I were studied. Fig. 7 (a) and (b) report the temporal evolution of emission intensity for $^1H_\alpha$ and Zr I and FWHM, respectively, in plasmas generated from a ^{1}H-loaded Zircaloy-4 target. All measurements were taken in 10 Torr He at ~0.5 mm from the target. This particular distance from the target was selected since closer to the target, $^1H_\alpha$ emission provides strong signal levels along with a narrower line profile. Emission intensity decays exponentially for both $^1H_\alpha$ and Zr I, although Zr I decays more rapidly. Linewidth (Fig. 7(b)) also follows an exponential decay behaviour, where the minimum measured FWHM is reached by ~ 1 µs after plasma onset.

Time-resolved electron densities were calculated from the Lorentzian width of $^1H_\alpha$ using the following relation[52]:

$$N_e = 8.02 \times 10^{12} \left(\frac{\Delta\omega_{1/2}}{\alpha_{1/2}}\right)^{3/2} [cm^{-3}] \qquad (3)$$

where N_e is electron density of $^1H_\alpha$ in cm^{-3}, $\Delta\omega_{1/2}$ is the Lorentzian width of the $^1H_\alpha$ in Å, and $\alpha_{1/2}$ is the half width of the reduced Stark profile, obtained from literature.[53] Electron density (reported in Fig. 8 for ^{1}H-containing Zircaloy-4) is found to decay exponentially with increasing time after plasma onset, from ~ 2.56 × 10^{16} cm^{-3} at ~50 ns to 6.65 × 10^{14} cm^{-3} at ~770 ns.

In addition to electron density and temperature, the line shapes and linewidths of spectral profiles in a plasma system are influenced by self-absorption.[54] The presence of self-absorption leads to an artificial increase in the measured linewidth typically seen in the analysis of $^1H_\alpha$ in a LIB plasma system. Although in prior works the $^1H_\beta$ (486.14 nm) line has been used to measure electron density since this line is less prone to self-absorption,[20, 54, 55] in this work the analysis of the $^1H_\beta$ (486.14 nm) line is not practical due to the crowded Zircaloy-4 spectrum, with several nearby Zr, Sn, Fe, and Cr lines. Self-absorption of the $^1H_\alpha$ line has been shown to significantly impact linewidths, and hence electron density measurements.[56]

e. Spatio-temporal evolution of plasma species

The kinetic distribution of species was studied using spatially and temporally resolved OTOF measurements to complement the analysis of time-resolved emission spectra previously presented (Fig. 7). OTOF measurements were performed for $^2H_\alpha$ and Zr I (471.01 nm). $^1H_\alpha$ and $^2H_\alpha$ showed similar kinetic distributions, hence $^2H_\alpha$ OTOF is only presented here. The Zr I line at 471.01 nm was selected since there are no overlaps with any other peaks of atoms or ions from other elements in the multi-component Zircalloy-4 plasma, and it is a relatively strong line compared to other Zr I lines in the visible spectrum. Fig. 9(a)-(b) reports the spatio-temporal distribution of $^2H_\alpha$ and Zr I species mapped by collecting OTOF data at various distances from the target.

As shown in Fig. 9, the kinetic distributions of $^2H_\alpha$ and Zr I are drastically different. The contour plots show that $^2H_\alpha$ emission occurs primarily closer to the target and at early times. In contrast, Zr I emits at farther distances with increased persistence compared to $^2H_\alpha$. This segregation is related to the requirement of higher temperature conditions for $^2H_\alpha$ emission compared to Zr I.

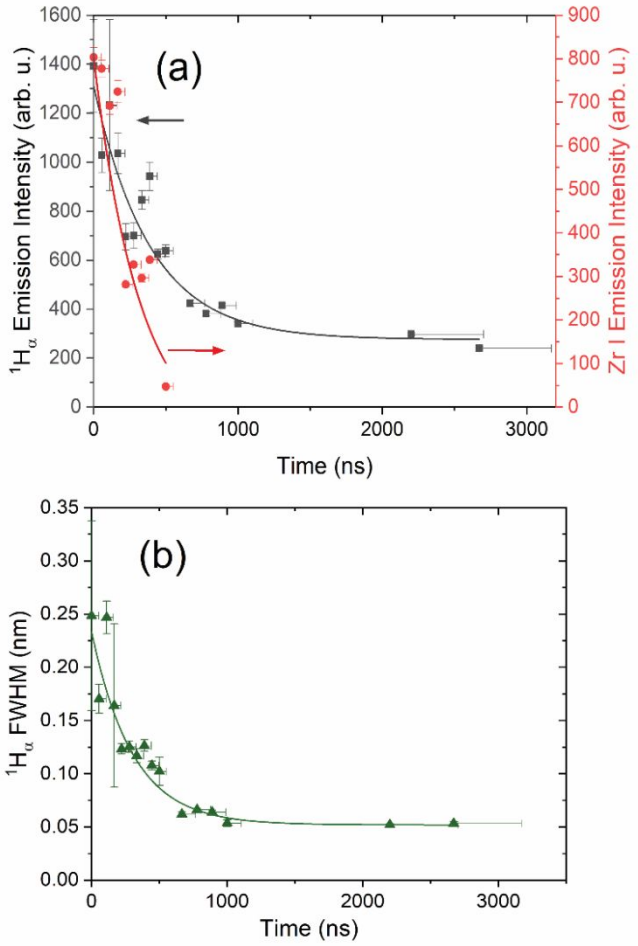

Fig. 7. Time-resolved (a) emission intensity for 1Hα and Zr I (655.05 nm), and (b) FWHM of $^1H_\alpha$ for a ^{1}H-loaded containing Zircaloy-4 target In 10 Torr He, at ~ 0.5 mm from the target. Gate width is given as the x-error bar for each data point.

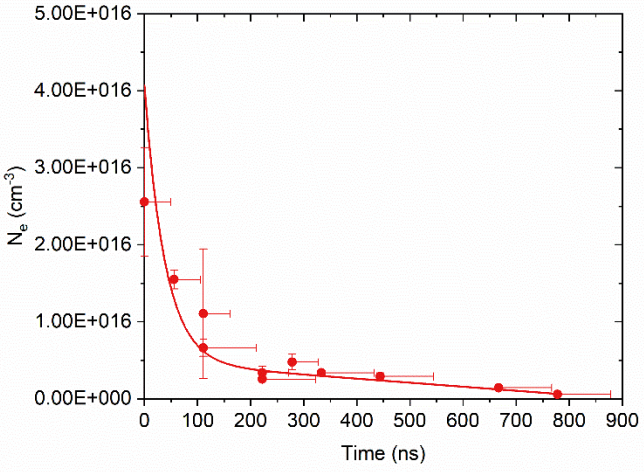

Fig. 8. Electron density as a function of time at ~0.5 mm from the target for ^{1}H-loaded Zircaloy-4 plasma in 10 Torr He. Gate width is given as the x-error bar for each data point.

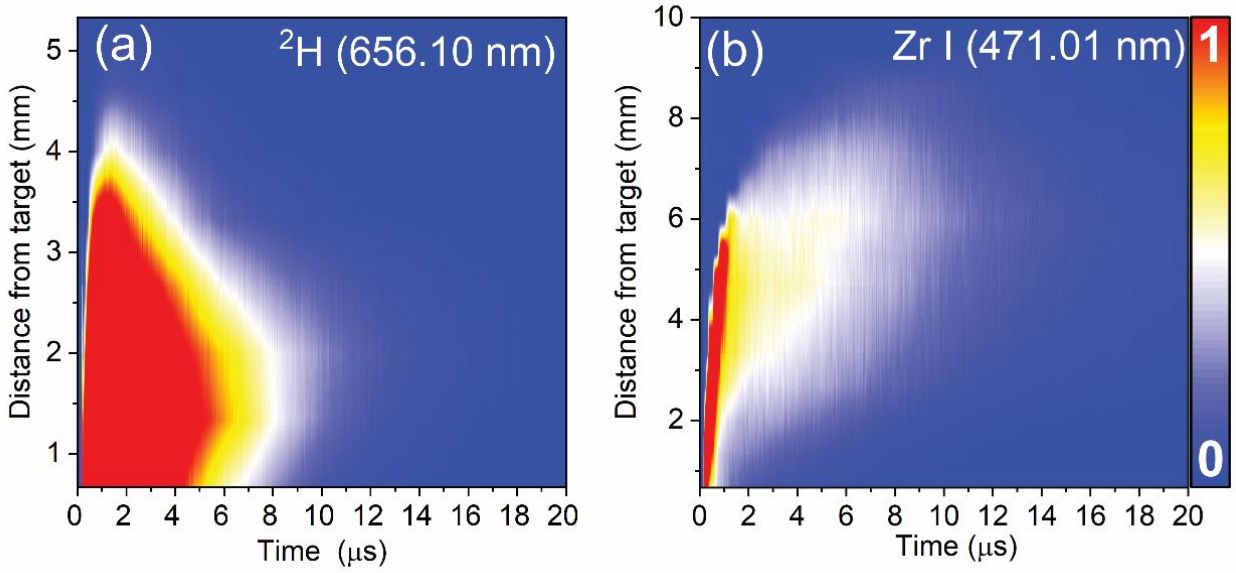

Fig. 9. Distance-time contour plots of OTOF data, illustrating spatio-temporal emission from (a) ^{2}H (656.10 nm) and (b) Zr I (471.01 nm). Each contour plot is normalized to its maximum intensity.

f. Comparison of $^2H_\alpha$ emission intensities for varying ^{2}H concentrations

Considering the pressure dependence, and temporal and spatial distribution of $^2H_\alpha$ and Zr I in femtosecond LIB plasmass, we analysed a series of ^{2}H-containing Zircaloy-4 samples with concentrations ranging from ~ 2 – 42 at. % ^{2}H (~6 - 15200 ppm by mass). Optical emission spectra were taken at a distance of ~ 0.5 mm from the target, 1 μs after plasma onset, with a 3 μs gate width in 10 Torr He. Position and timing for measurements were selected in order to obtain a strong emission signal, with minimal line broadening. Spectra were averaged over 8 shots after $^1H_\alpha$ and $^2H_\alpha$ emission reached a steady-state value (i.e., all ^{1}H surface contamination was removed). Three duplicate frames were saved per Zircaloy-4 sample so that an average and standard deviation of $^2H_\alpha$ emission intensity (calculated from area under a Voigt fit of the $^2H_\alpha$ curve) could be calculated and plotted versus known ^{2}H concentration (Fig. 10). This 'known' concentration was determined via weight gain measurements before and after the ^{2}H absorption process described in Experimental Details (section II). X error bars represent the error associated with the analytical balance. Y error bars represent the standard deviation between three duplicate $^2H_\alpha$ emission intensity measurements of 8 laser shots each. The linear fit given in Fig. 10 has a Pearson's correlation coefficient of ~0.98, and hence fits data well, although, only 5 data points are analysed here.

Unlike ns LA, the laser-target coupling during fs LA is extremely efficient, leading to high number density of atomic species in the plasma.[15, 46] Typically, high ablation efficiency is favourable in analytical applications since an increased signal from atomic lines can be achieved. However, this high ablation efficiency may be problematic in the case of analysing ^{1}H or ^{2}H emission signatures due to the possibility of self-absorption. To date, calibration curves for ^{1}H or ^{2}H have been reported for a range of concentrations, including: 200 ppm – 1000 ppm ^{2}H using 2 mJ ps laser pulsing focused onto a Zircaloy sample in 3 kPa (22.5 Torr) He gas,[26] ~ 10 ppm to 1600 ppm ^{2}H using 7 mJ ps laser focused onto a Zircaloy sample in 1.3 kPa (9.75 Torr) He gas,[40] up to 4300 ppm ^{1}H using 100 mJ ns laser focused onto Zircaloy sample in 760 Torr He gas, [57] and 0.5 - 20 at. % ^{2}H using a fs filament focused onto ^2H_2O-^1H_2O samples in Ar gas in atmospheric pressure (~760 Torr).[22] Each of these studies used different plasma generation conditions (i.e., ns, ps, fs-filament) in comparison to our work employing focused fs LA. Although the more efficient laser-target coupling and primarily atomic plume characteristic in fs laser induced plasmas may be favourable for depth profiling or detecting trace ^{1}H or ^{2}H, the self absorption of the $^1H_\alpha$ or $^2H_\alpha$ lines may be present for LIB plasmas produced for higher ^{1}H or ^{2}H concentrations than those studied here.

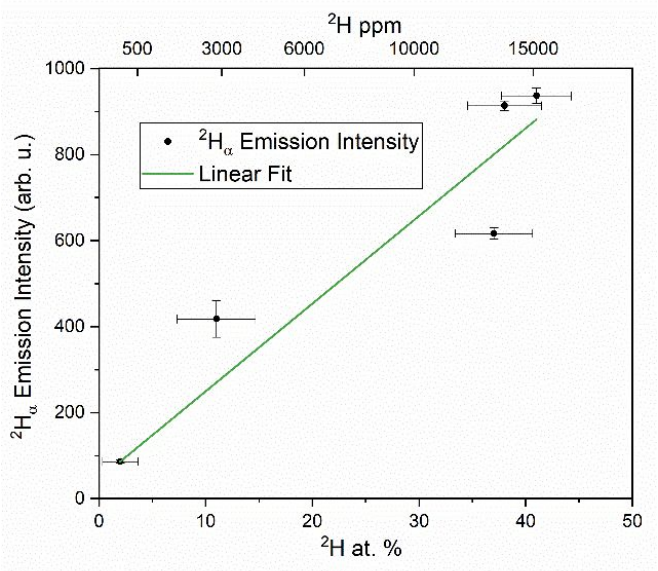

Fig. 10. $^2H_\alpha$ emission intensities versus measured ^2H concentration via weight gain measurements in Zircaloy-4 samples. Two x-axes for ^2H concentration are given: at. % and ppm by mass. The linear fit is described by the equation: $y = (20.39 \pm 2.21)x + (45.62 \pm 32.31)$.

IV. Conclusions

Femtosecond LIBS was used to analyse hydrogen isotopes (^1H and ^2H) in plasmas produced from Zircaloy-4 target materials with varying isotopic compositions (i.e., as-received, with ^1H, and with ^2H). A high purity He gas environment was used for all analyses due to its high thermal conductivity and low atomic weight, leading to efficient cooling of the LIB plasma. Spatially and temporally resolved emission spectral features were collected over a range of ambient gas pressures (~3-250 Torr) to explore emission features, line broadening, and plasma physical conditions.

This study highlights several considerations for the analysis of $^1H_\alpha$ and $^2H_\alpha$ in plasmas produced from multi-component targets via fs LIBS, including: (i) ^1H can be present as an impurity on the target surface and several cleaning shots should be performed prior to data collection, (ii) femtosecond LA in a moderate pressure ~10 Torr He ambient provides strong $^1H_\alpha$ emission signal, good SBR and SNR, relatively low electron density and thus minimal line broadening well-suited for analytical applications, (iii) emission spectra should be collected in a spatially-resolved manner and closer (~0.5 – 1 mm) to the target since $^{1,2}H_\alpha$ emission intensity is strongest in the hotter region of the LIB plasma, (iv) analysis of $^{1,2}H_\alpha$ should be performed at later times in LIB plasma evolution after electron density has decayed enough to provide minimal line broadening. We demonstrate that by implementing these considerations, a calibration curve relating $^2H_\alpha$ emission intensity to known ^2H concentration follows a linear relationship for a wide range of ^2H concentrations. Our findings from spatio-temporal analyses at varying pressures and times after plasma onset informed an experimental set-up that lead to line separation less than the isotopic shift, with strong emission intensity and good SBR and SNR, essential to the detection and analysis of ^1H, ^2H, and even ^3H via fs LIBS.

Conflicts of interest

There are no conflicts to declare.

Acknowledgements

The authors acknowledge the National Nuclear Security Administration (NNSA) Tritium Modernization Program for financially supporting this work. All work reported in this study was performed at Pacific Northwest National Laboratory, which is operated for the U.S. DOE by Battelle Memorial Institute under Contract No. DE-AC05-76RLO1830.

References

1. F. R. Doucet, G. Lithgow, R. Kosierb, P. Bouchard and M. Sabsabi, *Determination of isotope ratios using Laser-Induced Breakdown Spectroscopy in ambient air at atmospheric pressure for nuclear forensics*, *J Anal Atom Spectrom*, 2011, **26**, 536-541.
2. N. H. Thomas, B. L. Ehlmann, D. E. Anderson, S. M. Clegg, O. Forni, S. Schröder, W. Rapin, P. Y. Meslin, J. Lasue and D. M. Delapp, *Characterization of hydrogen in basaltic materials with Laser-Induced Breakdown Spectroscopy (LIBS) for application to MSL ChemCam data*, *Journal of Geophysical Research: Planets*, 2018, **123**, 1996-2021.
3. D. A. Cremers and R. C. Chinni, *Laser-induced breakdown spectroscopy—capabilities and limitations*, *Applied Spectroscopy Reviews*, 2009, **44**, 457-506.
4. A. T. Motta, L. Capolungo, L.-Q. Chen, M. N. Cinbiz, M. R. Daymond, D. A. Koss, E. Lacroix, G. Pastore, P.-C. A. Simon, M. R. Tonks, B. D. Wirth and M. A. Zikry, *Hydrogen in zirconium alloys: A review*, *Journal of Nuclear Materials*, 2019, **518**, 440-460.
5. D. Zhao, D. Wu, J. Oelmann, S. Brezinsek, Q. Xiao, R. Yi, L. Cai and H. Ding, *Highly depth-resolved characterization of fusion-related tungsten material based on picosecond laser-induced breakdown spectroscopy*, *J Anal Atom Spectrom*, 2020, **35**, 2867-2879.
6. S. Brezinsek, J. W. Coenen, T. Schwarz-Selinger, K. Schmid, A. Kirschner, A. Hakola, F. L. Tabarés, H. J. van der Meiden, M. L. Mayoral and M. Reinhart, *Plasma–wall interaction studies within the EUROfusion consortium: progress on plasma-facing components development and qualification*, *Nuclear fusion*, 2017, **57**, 116041.
7. S. Almaviva, L. Caneve, F. Colao, V. Lazic, G. Maddaluno, P. Mosetti, A. Palucci, A. Reale, P. Gasior and W. Gromelski, *LIBS measurements inside the FTU vessel mock-up by using a robotic arm*, *Fusion Engineering and Design*, 2020, **157**, 111685.
8. Y. S. Chen, D. Haley, S. S. A. Gerstl, A. J. London, F. Sweeney, R. A. Wepf, W. M. Rainforth, P. A. J. Bagot and M. P. Moody, *Direct observation of individual hydrogen atoms at trapping sites in a ferritic steel*, *Science*, 2017, **355**, 1196-1199.
9. S. Evers, C. Senöz and M. Rohwerder, *Hydrogen detection in metals: a review and introduction of a Kelvin probe*

approach, *Science and technology of advanced materials*, 2013, **14**, 014201.

10. G. Galbács, A. Kéri, I. Kálomista, É. Kovács-Széles and I. B. Gornushkin, *Deuterium analysis by inductively coupled plasma mass spectrometry using polyatomic species: An experimental study supported by plasma chemistry modeling*, *Analytica Chimica Acta*, 2020, **1104**, 28-37.
11. K. Li, J. Liu, C. R. M. Grovenor and K. L. Moore, *NanoSIMS imaging and analysis in materials science*, *Annual Review of Analytical Chemistry*, 2020, **13**, 273-292.
12. W. Jiang, W. G. Luscher, T. Wang, Z. Zhu, L. Shao and D. J. Senor, *A quantitative study of retention and release of deuterium and tritium during irradiation of γ-LiAlO2 pellets*, *Journal of Nuclear Materials*, 2020, **542**, 152532.
13. E. Kautz, J. Cliff, T. Lach, D. Reilly and A. Devaraj, *Correlating nanoscale secondary ion mass spectrometry and atom probe tomography analysis of uranium enrichment in metallic nuclear fuel*, *Analyst*, 2021, **146**, 69-74.
14. J. P. Singh and S. N. Thakur, *Laser-induced breakdown spectroscopy*, Elesiver, Amsterdam, 2020.
15. S. S. Harilal, J. R. Freeman, P. K. Diwakar and A. Hassanein, in *Laser-Induced Breakdown Spectroscopy*, Springer, 2014, pp. 143-166.
16. A. A. Bol'shakov, X. Mao, J. J. González and R. E. Russo, *Laser ablation molecular isotopic spectrometry (LAMIS): current state of the art*, *J Anal Atom Spectrom*, 2016, **31**, 119-134.
17. F. J. Fortes, J. Moros, P. Lucena, L. M. Cabalin and J. J. Laserna, *Laser-Induced Breakdown Spectroscopy*, *Anal Chem*, 2013, **85**, 640-669.
18. S. S. Harilal, B. E. Brumfield, N. L. LaHaye, K. C. Hartig and M. C. Phillips, *Optical spectroscopy of laser-produced plasmas for standoff isotopic analysis*, *Applied Physics Reviews*, 2018, **5**, 021301.
19. D. A. Cremers, A. Beddingfield, R. Smithwick, R. C. Chinni, C. R. Jones, B. Beardsley and L. Karch, *Monitoring Uranium, Hydrogen, and Lithium and Their Isotopes Using a Compact Laser-Induced Breakdown Spctroscopy (LIBS) Probe and High-Resolution Spectrometer*, *Applied Spectroscopy*, 2012, **66**, 250-261.
20. M. Burger, P. J. Skrodzki, L. A. Finney, J. Hermann, J. Nees and I. Jovanovic, *Isotopic analysis of deuterated water via single-and double-pulse laser-induced breakdown spectroscopy*, *Physics of Plasmas*, 2018, **25**, 083115.
21. K. H. Kurniawan, M. O. Tjia and K. Kagawa, *Review of Laser-Induced Plasma, Its Mechanism, and Application to Quantitative Analysis of Hydrogen and Deuterium*, *Applied Spectroscopy Reviews*, 2014, **49**, 323-434.
22. L. Genggeng, H. Huaming, R. Pengxu, Z. Yunlong and Z. Zhengye, *Calibration-free quantitative analysis of D/H isotopes with a fs-laser filament*, *J. Anal. At. Spectrom.*, 2020, **35**, 1320-1329.
23. Z. S. Lie, M. Pardede, E. Jobiliong, H. Suyanto, D. P. Kurniawan, R. Hedwig, M. Ramli, A. Khumaeni, T. J. Lie, K. H. Kurniawan, K. Kagawa and M. O. Tjia, *H-D Analysis Employing Low-Pressure microjoule Picosecond Laser-Induced Breakdown Spectroscopy*, *Anal Chem*, 2017, **89**, 4951-4957.
24. K. H. Kurniawan and K. Kagawa, *Hydrogen and Deuterium Analysis Using Laser-Induced Plasma Spectroscopy*, *Applied Spectroscopy Reviews*, 2006, **41**, 99-130.
25. H. Suyanto, Z. S. Lie, H. Niki, K. Kagawa, K. Fukumoto, H. Rinda, S. N. Abdulmadjid, A. M. Marpaung, M. Pardede and M. M. Suliyanti, *Quantitative analysis of deuterium in zircaloy using double-pulse laser-induced breakdown spectrometry (LIBS) and helium gas plasma without a sample chamber*, *Anal Chem*, 2012, **84**, 2224-2231.
26. M. Pardede, T. J. Lie, J. Iqbal, M. Bilal, R. Hedwig, M. Ramli, A. Khumaeni, W. S. Budi, N. Idris and S. N. Abdulmadjid, *H–D analysis employing energy transfer from metastable excited-state He in double-pulse LIBS with low-pressure He gas*, *Anal Chem*, 2018, **91**, 1571-1577.
27. Z. S. Lie, M. Pardede, R. Hedwig, M. M. Suliyanti and E. Steven, *Maliki, KH Kurniawan, M. Ramli, SN Abdulmadjid, N. Idris, K. Lahna, K. Kagawa, MO Tjia.''Intensity Distributions of Enhanced H Emission from Laser-Induced Low-Pressure He Plasma and a Suggested He-Assisted Excitation Mechanism''*, *J. Appl. Phys*, 2009, **106**, 043303.
28. R. E. Russo, A. A. Bol'shakov, X. Mao, C. P. McKay, D. L. Perry and O. Sorkhabi, *Laser Ablation Molecular Isotopic Spectrometry*, *Spectrochimica Acta Part B: Atomic Spectroscopy*, 2011, **66**, 99-104.
29. P. Ran, G. Li and H. Hou, *Laser ablation molecular isotopic spectrometry for analysis of OD/OH isotopologues in plasma*, *Spectrochimica Acta Part B: Atomic Spectroscopy*, 2021, **179**, 106093.
30. E. J. Kautz, A. Devaraj, D. J. Senor and S. S. Harilal, *Hydrogen isotopic analysis of nuclear reactor materials using ultrafast laser-induced breakdown spectroscopy*, *Optics Express*, 2021, **29**, 4936-4946.
31. S. Imashuku, T. Kamimura, S. Kashiwakura and K. Wagatsuma, *Quantitative Analysis of Hydrogen in High-Hydrogen-Content Material of Magnesium Hydride via Laser-Induced Breakdown Spectroscopy*, *Anal. Chem.* , 2020, **92**, 11171–11176.
32. S. S. Harilal, P. K. Diwakar and G. Miloshevsky, in *Laser-Induced Breakdown Spectroscopy (Second Edition)*, eds. J. P. Singh and S. N. Thakur, Elsevier, Amsterdam, 2020, pp. 139-166.
33. M. Ying, X. Wang, W. Cheng, B. Liao and X. Zhang, *Time-of-flight spectroscopy characterization of the plasma plume from a laser-ablated potassium titanyl phosphate crystal*, *Physica B: Condensed Matter*, 2015, **466**, 96-100.
34. N. Smijesh, K. Chandrasekharan, J. C. Joshi and R. Philip, *Time of flight emission spectroscopy of laser produced nickel plasma: Short-pulse and ultrafast excitations*, *Journal of Applied Physics*, 2014, **116**, 013301.
35. V. Sivakumaran, H. C. Joshi, R. K. Singh and A. Kumar, *Optical time of flight studies of lithium plasma in double pulse laser ablation: Evidence of inverse Bremsstrahlung absorption*, *Physics of Plasmas*, 2014, **21**, 063110.
36. M. Skočić, D. Dojić and S. Bukvić, *Consideration of optical time of flight measurement in laser induced plasmas*, *Spectrochimica Acta Part B: Atomic Spectroscopy*, 2020, **165**, 105786.
37. J. P. Zheng, Z. Q. Huang, D. T. Shaw and H. S. Kwok, *Generation of high-energy atomic beams in laser-superconducting target interactions*, *Applied Physics Letters*, 1989, **54**, 280-282.
38. S. Djurović, D. Nikolić, I. Savić, S. Sörge and A. V. Demura, *Asymmetry of H β Stark profiles in T-tube hydrogen plasma*, *Physical Review E*, 2005, **71**, 036407.

39. W. L. Wiese, D. E. Kelleher and D. R. Paquette, *Detailed Study of the Stark Broadening of Balmer Lines in a High-Density Plasma*, *Physical Review A*, 1972, **6**, 1132-1153.
40. A. M. Marpaung, Z. S. Lie, H. Niki, K. Kagawa, K.-i. Fukumoto, M. Ramli, S. N. Abdulmadjid, N. Idris, R. Hedwig and M. O. Tjia, *Deuterium analysis in zircaloy using ps laser-induced low pressure plasma*, *Journal of Applied Physics*, 2011, **110**, 063301.
41. S. S. Harilal, N. Farid, J. F. Freeman, P. K. Diwakar, N. L. LaHaye and A. Hassanein, *Background gas collisional effects on expanding fs and ns laser ablation plumes*, *Applied Physics A*, 2014, **117**, 319.
42. E. J. Kautz, J. Yeak, B. E. Bernacki, M. C. Phillips and S. S. Harilal, *The role of ambient gas confinement, plasma chemistry, and focusing conditions on emission features of femtosecond laser-produced plasmas J Anal Atom Spectrom*, 2020, **35**, 1574-1586.
43. E. J. Kautz, M. C. Phillips and S. S. Harilal, *Unraveling spatio-temporal chemistry evolution in laser ablation plumes and its relation to initial plasma conditions*, *Anal Chem*, 2020, **92**, 13839-13846.
44. *R. L. Kurucz atomic linelist*, Harvard-Smithsonian Center for Astrophysics, 2011.
45. N. Farid, S. S. Harilal, H. Ding and A. Hassanein, *Emission features and expansion dynamics of nanosecond laser ablation plumes at different ambient pressures*, *Journal of applied physics*, 2014, **115**, 033107.
46. J. R. Freeman, S. S. Harilal, P. K. Diwakar, B. Verhoff and A. Hassanein, *Comparison of optical emission from nanosecond and femtosecond laser produced plasma in atmosphere and vacuum conditions*, *Spectrochimica Acta Part B: Atomic Spectroscopy*, 2013, **87**, 43-50.
47. H.-J. Kunze, *Introduction to plasma spectroscopy*, Springer, Heidelburg, 2009.
48. L. W. Anderson, F. M. Pipkin and J. C. Baird Jr, *Hyperfine structure of hydrogen, deuterium, and tritium*, *Physical Review*, 1960, **120**, 1279.
49. A. E. Kramida, *A critical compilation of experimental data on spectral lines and energy levels of hydrogen, deuterium, and tritium*, *Atomic Data and Nuclear Data Tables*, 2010, **96**, 586-644.
50. V. I. Korobov, J. C. J. Koelemeij, L. Hilico and J. P. Karr, *Theoretical Hyperfine Structure of the Molecular Hydrogen Ion at the 1 ppm Level*, *Physical Review Letters*, 2016, **116**, 053003.
51. H. A. Bethe and E. E. Salpeter, *Quantum mechanics of one- and two-electron atoms*, Springer Science & Business Media, 2012.
52. A. M. El Sherbini, H. Hegazy and T. M. El Sherbini, *Measurement of electron density utilizing the Hα-line from laser produced plasma in air*, *Spectrochimica Acta Part B: Atomic Spectroscopy*, 2006, **61**, 532-539.
53. P. Kepple and H. R. Griem, *Improved Stark Profile Calculations for the Hydrogen Lines hydrogen lines H α, H β, H γ, and H δ*, *Physical Review*, 1968, **173**, 317-325.
54. H. R. Griem, J. Halenka and W. Olchawa, *Comparison of hydrogen Balmer-alpha Stark profiles measured at high electron densities with theoretical results*, *Journal of Physics B: Atomic, Molecular and Optical Physics*, 2005, **38**, 975.
55. N. Konjević, M. Ivković and N. Sakan, *Hydrogen Balmer lines for low electron number density plasma diagnostics*, *Spectrochimica Acta Part B: Atomic Spectroscopy*, 2012, **76**, 16-26.
56. C. G. Parigger, C. M. Helstern and G. Gautam, *Laser-plasma and self-absorption measurements with applications to analysis of atomic and molecular stellar astrophysics spectra*, *Atoms*, 2019, **7**, 63.
57. M. Ramli, K.-i. Fukumoto, H. Niki, S. N. Abdulmadjid, N. Idris, T. Maruyama, K. Kagawa, M. O. Tjia, M. Pardede and K. H. Kurniawan, *Quantitative hydrogen analysis of zircaloy-4 in laser-induced breakdown spectroscopy with ambient helium gas*, *Applied optics*, 2007, **46**, 8298-8304.